Dynamic centrifugal model test for unsaturated embankments considering seepage flow and the numerical analysis

Expérimentation en centrifugeuse et modélisation numérique de la réponse aux séismes de remblais non saturés en prenant en compte l'écoulement

Higo Y., Oka F., Kimoto S., Kinugawa T.
Department of Civil and Earth Resources Engineering, Kyoto University, Japan

Lee C.-W., Doi T.
Former graduate student of Department of Civil and Earth Resources Engineering, Kyoto University, Japan

ABSTRACT: Earthquake-induced failure of unsaturated road embankments has taken place during the past earthquakes. It has been pointed out that water flow or higher water content of road embankments was a possible reason of the damage. In this study, dynamic resistance of unsaturated embankments with and without the seepage flow has been studied through the centrifugal model tests of unsaturated embankment and their numerical simulations by a multi-phase coupled finite element method with an elasto-plastic constitutive model. During the tests, displacement, pore pressures, and acceleration of embankments have been fully monitored. The dynamic behavior of unsaturated embankments with infiltration of pore water has been discussed on the basis of comparison between the experimental and the numerical results. From the present study, we have found that the seepage flow and the high water content extensively affect the dynamic stability of unsaturated road embankments.

RÉSUMÉ: Les remblais routiers non saturés peuvent s'écrouler lors d'un séisme, la cause de cet écroulement étant sans doute à rechercher dans l'écoulement d'eau ou dans des grandes valeurs de teneur en eau au sein du remblai. Dans cet article, la résistance dynamique d'un remblai non saturé est étudiée, avec ou sans écoulement, par des essais en centrifugeuse et par leur modélisation numérique aux Eléments Finis, en utilisant une approche hydromécanique couplée et un modèle constitutif élasto-plastique pour le sol. Les déplacements, les pressions interstitielles et les accélérations ont été mesurés tout au long des essais. Les résultats expérimentaux et les résultats numériques ont été comparés. Les résultats de cette étude confirment que l'écoulement et la forte teneur en eau ont effectivement un rôle majeur pour la stabilité dynamique des remblais routiers non saturés.

KEYWORDS: unsaturated soil, embankment, earthquake, failure, dynamic centrifugal model test, numerical simulation.

1 INTRODUCTION

It is well known that the road embankment is still vulnerable against earthquakes. Earthquakes damaged road embankments during the extensive earthquakes such as the 2011 off the Pacific Coast of Tohoku Earthquake (M9.0). In particular, road embankments constructed on mountain/hill sides were severely damaged by the 2009 Suruga Bay Earthquake, the 2007 Noto Hanto Earthquake and the 2004 Niigata-ken Chuetsu Earthquake etc.

In the cases of the Noto Hanto Earthquake and the Niigata-ken Chuetsu Earthquake, seepage water flow or higher water content in the embankments was a possible reason of the damage of the road embankments. Increase in the water contents causes loss of the inter-particle force caused by suction and decrease in the skeleton stress. This suggests that the effect of the seepage water flow and the high water content in the embankments on the dynamic failure of road embankment has to be studied in detail. However, to the authors' knowledge, there are a limited number of physical model studies on unsaturated embankments considering seepage water as well as numerical ones (e.g., Hayashi et al. 2002, Doi et al. 2010).

In this study, seismic resistance of unsaturated embankments with and without the seepage water has been studied through the centrifugal model tests and their numerical simulations by a multi-phase coupled finite element method with an elasto-plastic constitutive model (Oka et al. 2008, Oka et al. 2011). The dynamic behavior of unsaturated embankments with infiltration of the pore water has been discussed on the basis of comparison between the experimental and numerical results.

2 DYNAMIC CENTRIFUGAL MODEL TESTS

2.1 *Soil used in the test*

The soil used in the model tests is Yodogawa-levee sand, which has been used to fix the embankment of Yodo River in Kansai area. The physical properties of Yodogawa-levee sand are listed in Table 1.

Table 1. Physical properties of Yodogawa-levee sand

Parameter	***Value***
Sand content (%)	73.2
Silt content (%)	14.7
Clay content (%)	12.1
D_{max} (mm)*	2.0
D_{50} (mm)	0.29
ρ_s (g/cm^3)	2.661
w_{opt} (%)	13.7
ρ_{dmax} (g/cm^3)	1.861
k(m/sec)**	4.79×10^{-6}

*Maximum diameter of sieved particle
**Permeability when degree of compaction is 90%

2.2 *Testing procedure*

The model configuration and the sensor locations are illustrated in Fig. 1. Prior to preparing the specimen, test samples were mixed with water to set up the initial water contents of 15%. Then, model embankments were prepared by compacting method in eight layers; the base ground and the embankment were separated into three layers (thickness: 30mm, 15mm, 15mm), and five layers (as same thickness: 20mm), respectively. During the model construction, the accelerometers and the pore pressure transducers were embedded at the prescribed locations. The degree of compaction of all the cases

was set to be 90%. After construction of the embankment, laser displacement sensors were installed at the prescribed locations. In addition, the targets were inserted in each compacted layer, for quantifying the displacements between before and after the tests by PTV (Particle Tracking Velocimetry) technique. The centrifugal gravity used in this study was 50G.

The infiltration of water has been performed from the three slits of the right side wall (see Figure 1). The water of 2,000mL was prepared in the water supply tank attached on the model container. The water level of the tank was set to be 6.75m. The valves of the three slits installed on the wall with the height of 1.5m, 3m, and 4.5m from the bottom were opened and the water flowed into the model embankment and the base ground through the slits. In the present study, the water was used as the pore fluid, whereas viscous fluids with the 50 times viscosity of water, e.g., metolose solution, are often used for satisfying the similarity rule. This is because the matric suction of the metolose solution is smaller than that of the water. Note that the permeability of the embankment is 50 times in 50G field.

The centrifuge was spun up to an acceleration of 50G and seepage in 50G field was started. The water level was increased and reached close to the steady state, dynamic loads was applied to the model embankment. The tapered sine waves with a frequency of 1 Hz and an amplitude of approximately 400 gal were used as an input wave, and the duration of the wave was 30 seconds.

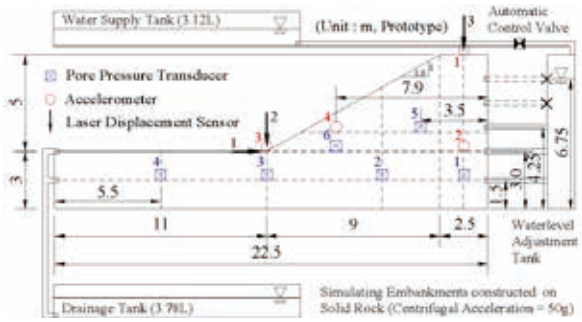

Figure 1. Model embankment and arrangement of sensors

2.3 *Testing program*

Two dynamic centrifugal model tests were performed. One has been conducted without infiltration (Case 1), and the other has been done with the seepage flow (Case 2). Average water content measured after the test was 12.7% in Case 1, which is similar to the optimum water content.

2.4 *Test results*

Figure 2 demonstrates a time profile of the pore water pressure at the base ground during the infiltration process and the water level estimated by the pore water pressure. All of the experimental results are expressed in a prototype scale hereinafter. It is seen that the pore water pressures were increased induced by the infiltration of water and reached almost steady state after 12 hour. The seepage area is shown in Figure 3 obtained in the other test with the same testing conditions as Case 1 other than the use of the yellow colored water. It is seen that the seepage area is wider than that estimated by the pore water pressures as shown in Figure 2. This indicates that the unsaturated seepage flow occurs in the specimen.

Figure 4 shows the distribution of displacement vector, and Table 2 shows the displacements at the toe of the slope and the crest. Displacement in Case 2 is much larger than Case 1 due to the effect of infiltration. This suggests that an increase of the pore water pressure by infiltration causes the decrease in suction and the skeleton stress of the embankment.

Time profiles of the excess pore water pressure measured under the crest (No.1) and in the base ground (No. 4) are shown in Figure 5. Note that the pore water pressure at the beginning of the loading is shifted to zero. While the excess pore water pressure levels in Case 1 are almost zero, those in Case 2 are rather high. In particular, it is possible that liquefaction occurs because the pore pressure of P4 at the base ground of Case 1 increases up to the initial vertical stress.

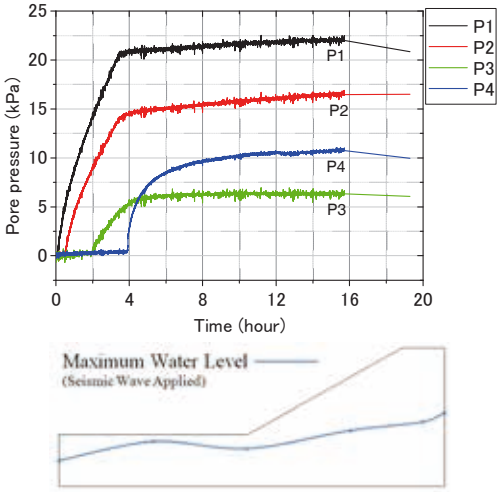

Figure 2 Time profile of pore water pressure and the water level estimated by the pore water pressure (Case 2)

Table 2. Displacements after the tests

Case	*Toe of the Slope*		*Crest*
	x	*y*	*y*
1	-0.4	7.1	0.2
2	-213.0	24.0	-380.0

* x: horizontal displacement, y: vertical displacement (in prototype, unit: mm)

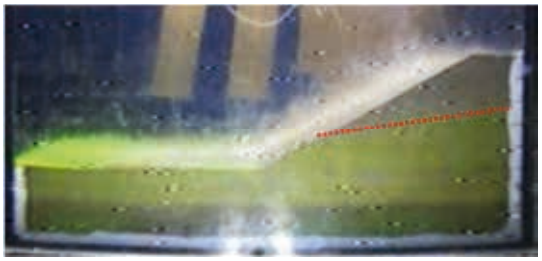

Figure 3. Seepage area indicated by yellow colored water

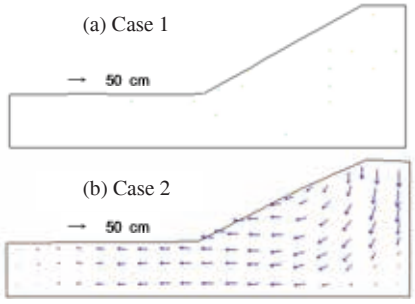

Figure 4. Distribution of the displacement vectors

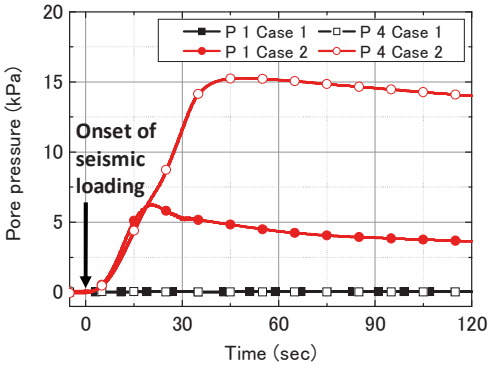

Figure 5. Excess pore water pressure-time profile

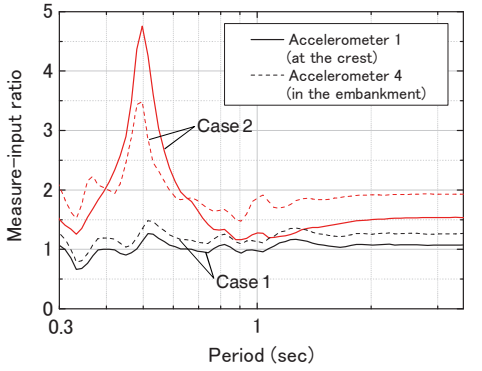

Figure 6. Acceleration response spectrum (measured-input ratio)

Fig. 6 shows the acceleration response spectrum, namely, measured-input ratio, calculated using the EMPR program developed by Sugito et al. (2000) at the crest and in the embankment. Damping parameter used in this analysis is 0.05. The higher amplification occurs in Case 2 than Case 1, and the predominant period is about 0.5sec. This is probably because of the reduction in the strength and the stiffness of the embankment due to the infiltration.

3 NUMERICAL SIMULATION OF THE DYNAMIC CENTRIFUGAL MODEL TESTS

3.1 *Multi-phase coupled liquefaction-analysis method for elasto-plastic unsaturated soils*

In the formulation of the dynamic coupled analysis, the simplified three-phase method is used in which the compressibility of air is assumed to be very high, whereas the soil particle and the pore water are incompressible as compared with the air (Oka et al. 2007, 2008, Kato et al. 2009), namely, the three-phase method can be simplified into the soil-water coupled two-phase mixture theory. A cyclic elasto-plastic model based on the non-linear kinematic hardening rule (Oka et al., 1999) was used in the analysis with a modified plastic dependency of the modulus, into which the non-linear hardening rule was incorporated. As the stress variable of the constitutive model, the skeleton stress is used in order to describe the mechanical behavior of unsaturated soils (e.g., Oka et al. 2007, 2008, Oka and Kimoto 2012). Skeleton stress tensor σ'_{ij} is defined as follows:

$$\sigma'_{ij} = \sigma_{ij} + P^F \delta_{ij}\ ,\ P^F = S_r p^W + (1 - S_r) p^G \qquad (1)$$

where σ_{ij} is the total stress tensor, δ_{ij} is Kronecker's delta, P^F is the average fluid pressure, p^W is the pore water pressure, p^G is the pore air pressure, and S_r is the degree of saturation. For the full description of the behavior of unsaturated soil, it is necessary to incorporate the suction in the constitutive model.

A u-p formulation for the liquefaction analysis (Oka et al., 2004) is adopted to solve the governing equations, in which the displacement of the solid phase and the pore pressure are used as independent variables. In the present analysis, the finite element method was used for the spatial discretization of the equation of motion for the whole mixture, and the finite difference method was used for the discretization of the continuity equation for the water phase.

3.2 *Analysis model and the boundary conditions*

Figure 7 shows the analysis model of the embankment and the finite element meshes used in the analysis. The embankment is initially unsaturated with an initial suction of 3.21 kPa corresponding to the initial degree of saturation of 67.8%. The right boundary is partly drainage one in order to simulate the water supply with the hydrostatic pressure. After the simulation of the water infiltration for 24 hours, dynamic analysis with the same input wave as in the experiment has been performed. Material parameters used in this analysis are listed in Table 3. The permeability coefficients of the elements just close to the drainage boundary are 10 times lower than the other parts because the water is likely to flow between the soil and the wall of the model container. The bulk modulus of the pore fluid of 5,000 kPa is lower than that of the water in order to model the mixture of the pore water and the pore air since the unsaturated seepage flow was observed in the experiment.

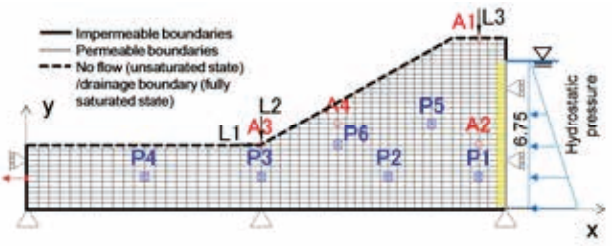

Figure 7 Analysis model and the boundary conditions

Table 3 Material parameters

Initial void ratio e_0	0.589
Compression index λ	0.0804
Swelling index κ	0.0001
Elastic shear modulus G_0/σ'_{m0}	4000
Permeability k (m/s)	4.79×10^{-4}
Bulk modulus of pore fluid K^f (kPa)	6000
Phase transformation stress ratio M^*_m	1.270
Failure stress ratio M^*_f	1.270
Kinematic hardening parameter B^*_0	10000
Kinematic hardening parameter B^*_1	150
Kinematic hardening parameter C_f	50
Quasi-overconsolidation ratio	1.3
Anisotropy parameter C_d	2000
Dilatancy coefficient D^*_0	1.0
Dilatancy coefficient n	2.0
Referential strain parameter γ^{P*}_r	0.008
Referential strain parameter γ^{E*}_r	0.08
van Genuchten's parameter α (1/m)	19.6
van Genuchten's parameter n'	1.2

3.3 *Simulation results*

Figure 8 shows the time profile of the pore water pressure during the seepage process. Comparing with the test results shown in Figure 2, the pore water pressure level at P1, P2, and P3 of the simulation results are higher than those of the test results. Meanwhile, the seepage area shown in Figure 9 is almost the same as that observed in the test (Figure 3). Namely, the unsaturated seepage flow was observed in experiment, while the fully saturated flow is obtained by this analysis. In this analysis, the unsaturated seepage flow has been modeled by the reduction of the bulk modulus of the pore fluid.

Displacements-time profile at the toe and the crest obtained by the analysis are in good agreement with the test results as shown in Figure 10. Figure 11 shows the distribution of γ^p at the end of the dynamic loading, in which $\gamma^p = \int (de_{ij}^p de_{ij}^p)^{1/2}$ (de_{ij}^p: plastic deviatoric strain increment). It can be seen that the several strain localization zones appear from the toe of the embankment to the crest. In addition, another strain localization zone can be seen in the base ground, which is consistent with the test results (Figure 4).

The distribution of pore water pressure is shown in Figure 12. It is seen that the pore water pressure increases in the seepage area. Figure 13 shows the skeleton stress decreasing ratio SSDR (defined as $1 - \sigma_m'/\sigma_{m0}'$, σ_m': current mean skeleton stress, σ_{m0}': initial mean skeleton stress) at the end of the dynamic loading. The higher SSDR is observed just below the toe of the embankment. This suggests that the decrease in the mean skeleton stress due to the increase in pore pressure induces the large deformation of the embankment with water infiltration.

4 CONCLUSIONS

Dynamic behaviors of unsaturated embankment considering seepage flow have been studied through the centrifugal model tests and their numerical simulation. For the seepage process, the unsaturated seepage flow has been observed in the experiment, and the seepage area of numerical simulation has been similar to that of experiment. It is found in the dynamic loading process that the infiltration of water into the unsaturated embankment has induced the large deformation in the seepage area due to the generation of pore water pressure in the embankment. The numerical results have provided that the increase in the pore pressure leads to the decrease in the mean skeleton stress in the seepage area, in particular, just below the toe of the embankment.

5 ACKNOWLEDGEMENTS

This research was supported in part by the National Institute for Land and Infrastructure Management, MLIT, Japan (Grant for research and development of technologies for improving the quality of road policy, No. 21-4, 2009-2012).

6 REFERENCES

Doi, T., Higo, Y., Oka, F., Kimura, M., Kimoto, S. & Lee, C.-W., Proceedings of 23rd KKCNN 2010, Taipei, pp. 303-306, 2010.

Hayashi, H., Nishikawa, J. & Egawa, T., Proc. Int. Conf. Physical Modelling in Geotechnics, ICPMG '02, Phillips, R., et al., eds., pp. 483-488, 2002.

Kato, R., Oka, F., Kimoto, S., Kodaka, T. & Sunami, S., Journal of Geotechnical Engineering, JSCE, 65 (1), 226-240, 2009 (in Japanese).

Oka, F., Yashima, A., Tateishi, A., Taguchi, T. & Yamashita, S., Géotechnique, 49(5), 661-680, 1999.

Oka, F., Kodaka, T. & Kim Y.-S., Int. J. Numer. Anal. Meth. Geomech., 28 (2), 131-179, 2004.

Oka, F., Kodaka, T., Kimoto, S., Kato, R. & Sunami, S., Key Engineering Materials, 340-341, pp.1223-1230, 2007.

Oka, F., Kimoto, S., Kato, R., Sunami, S. & Kodaka, T., Proc. 12th Int. Conf. IACMAG, Singh, D.N. ed., 2029-2041, 2008.

Oka, F., Kimoto, S. and Kato, R., First International Conference on Geotechnique, Construction Material and Environment, Mie, Japan, pp.15-22, 2011.

Oka, F. and Kimoto, S., Computational modeling of multiphase geomaterials, CRC Press, Taylor and Francis Group, 2012.

Sugito, M., Furumoto, Y., & Sugiyama, T., 12th World Conference on Earthquake Engineering, 2111/4/A CD-ROM, Auckland, New Zealand, 2000.

.

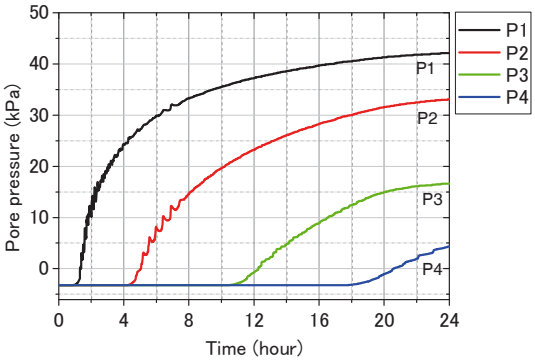

Figure 8. Pore water pressure-time profile during the seepage process

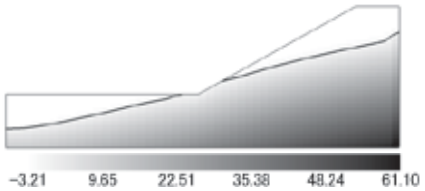

Figure 9. Distribution of pore water pressure at 24 hours of the seepage process (unit: kPa)

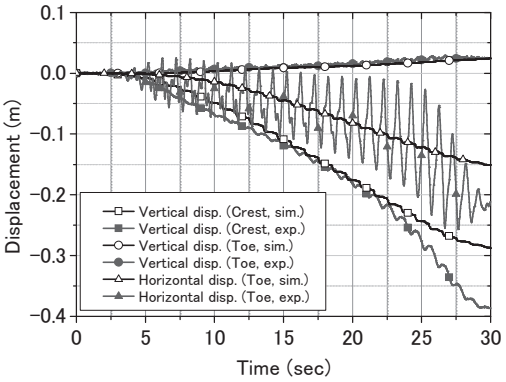

Figure 10. Displacements-time profile during the dynamic loading process

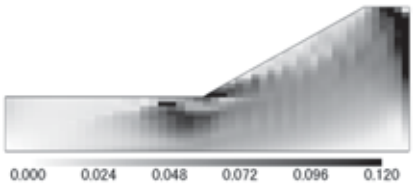

Figure 11 Distribution of γ^p at 30 seconds of the dynamic loading process (max: 0.240)

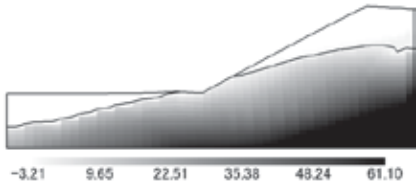

Figure 12 Distribution of the pore water pressure at 30 seconds of the dynamic loading process (Unit: kPa, max: 109.0kPa)

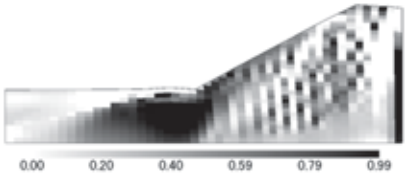

Figure 13 Distribution of SSDR at 30 seconds of the dynamic loading process